Intermetallics 121 (2020) 106775

Contents lists available at ScienceDirect

Intermetallics

journal homepage: http://www.elsevier.com/locate/intermet

Tensile creep behavior of an equiatomic CoCrNi medium entropy alloy

Di Xie [a], Rui Feng [a], Peter K. Liaw [a], Hongbin Bei [b,**], Yanfei Gao [a,*]

[a] Department of Materials Science and Engineering, University of Tennessee, Knoxville, TN, 37996, USA
[b] School of Materials Science and Engineering, Zhejiang University, Hangzhou, 310058, PR China

ARTICLE INFO

Keywords:
Medium entropy alloy
Creep deformation
Creep lifetime
Dislocation climb
Stacking fault
Temperature dependence

ABSTRACT

Tensile creep behavior of the CoCrNi medium entropy alloy in a temperature range of 973–1073 K was investigated in this study. According to the fitted stress exponent and activation energy, dislocation climb and lattice diffusion are proposed to be the dominated creep deformation mechanism for this alloy. During creep tests, the plate-like Cr-rich σ phase forms along the grain boundaries of the originally single-phase face-centered-cubic (FCC) CoCrNi alloy. It is suggested that low stacking-fault energy and local chemical ordering be responsible for the superior creep resistance and lifetime as opposed to that of the CoCrFeMnNi alloy.

1. Introduction

Equiatomic alloys, which generally consist of five or more principal elements and often called high entropy alloys (HEAs), have attracted extensive attention because of their unique mechanical properties [1,2]. Different from traditional alloys, HEAs derive their properties from multi-principal elements, which arrange in a simple lattice structure, instead of from one or two base elements. Recently the temperature dependence of the strength and hardness of HEAs has been recently widely investigated [3–5]. However, reports on the creep behavior of HEAs are limited. The investigation on the creep behavior of $Al_xCoCrFeNi$ (x = 0.15, 0.60) alloys using the stress relaxation method at 853–973 K [6] demonstrated the cross-slip dominated deformation mechanism and a lower creep resistance for higher Al content alloy due to its higher stacking fault energy. Dobeš et al. [7] found that yttrium-rich nano-sized oxide particles have significantly improved the creep behavior of CoCrFeMnNi HEA at a temperature range from 973 K to 1073 K due to the higher degree of effective grain boundary and dislocation pinning effects [8]. Cao et al. [9] proposed that the creep behavior of CoCrFeMnNi HEA exhibits a stress-dependent transition from a low-stress region (LSR-region I) to a high-stress region (HSR-region II) at a temperature range from 773 K to 873 K with an average grain size of 25 μm. Kang et al. [10] found the transition of creep mechanism from dislocation creep to glide in CoCrFeMnNi alloy and proposed the significant importance of Cr element on the viscous glide of dislocations at high stresses.

The subset of CoCrFeMnNi alloy, including equiatomic quinary, quaternary, and ternary single FCC solid-solution alloys, has been systematically investigated, exhibiting excellent strength and ductility combination [11,12]. The ternary CoCrNi medium entropy alloy (MEA) exhibits the most superior mechanical properties, including strength and ductility at the temperature range from 77 K to 673 K [12]. The superiority of CoCrNi out of all other subsets can be rationalized from the largest mismatches in atomic size and modulus according to the Labusch model for solid solution strengthening. Motivated by these results, in this paper, the creep behavior of CoCrNi MEA is carefully investigated. Due to the compositional and microstructural simplicity, CoCrNi alloy can serve as a bridge linking between the conventional binary alloys and the relatively less understood HEAs, which will offer fundamental understanding and design strategy for the novel materials for high temperature applications.

2. Experimental procedures

In this work, CoCrNi buttons were fabricated by arc-melting and re-melted at least five times. Rectangular ingots with a dimension of 12.7 mm × 25.4 mm × 127 mm were obtained by drop-casting into copper molds, followed by homogenized for 24 h at 1473 K and water quenching. Then cold rolling was applied along the longitudinal ingot direction to a total thickness reduction of 92% without cross-rolling or intermediate annealing. Dog-bone specimens with gauge dimensions of ϕ3.175 mm × 28 mm were cut from the cold rolling sheets by electrical

* Corresponding author.
** Corresponding author.
E-mail addresses: hbei2018@zju.edu.cn (H. Bei), ygao7@utk.edu (Y. Gao).

https://doi.org/10.1016/j.intermet.2020.106775
Received 20 January 2020; Received in revised form 7 March 2020; Accepted 16 March 2020

discharge machining (EDM) with longitudinal axes parallel to the rolling direction, sealed in vacuum-quartz tubes, and subsequently annealed at 1373 K for 2 h to remove the deformation substructure from cold rolling and achieve equiaxed grain structures. The gauge sections of these samples were mechanically polished using 800-grit SiC paper before the mechanical test. Tensile creep tests were performed under constant load mode at 973 K, 1023 K, and 1073 K, respectively.

TEM characterization was performed on ZEISS LIBRA 200 HT FE MC. Thin foils for the TEM observations were taken from the gauge section of crept/ruptured samples. The TEM thin foils were prepared by twin-jet polishing, using an electrolyte consisting of 95% (volume percent) ethanol and 5% perchloric acid in a volume fraction at a temperature of -40 °C and an applied voltage of 30 V.

3. Results

3.1. Initial microstructures

The microstructure of the annealed ternary CoCrNi alloy prior to high-temperature creep deformation is shown in Fig. 1. The mean grain size is approximately 149 ± 4 μm as determined by electron backscattered diffraction (EBSD). The distribution of alloying elements was examined using energy dispersive spectroscopy (EDS) maps. The chemical component of this alloy after annealing is determined to be ~33.37 at.% Cr, ~33.66 at.% Co, and ~32.97 at.% Ni. According to the backscattered electron (BSE) scanning-electron microscopy (SEM) image and the corresponding EDS elemental maps, as shown in Fig. 1 (b–e), Co, Cr, and Ni elements are uniformly distributed in the microstructure without the observation of segregation of alloying elements and additional phases. Meanwhile, X-ray diffraction (XRD) result in Fig. 1(f) shows a single FCC phase without any intermetallic compounds after annealing treatment, consistent with our previous results [11,12].

3.2. Steady-state deformation behavior

Representative strain-time curves of CoCrNi alloy at 70 MPa are given in Fig. 2 (a), which present the typical primary creep, steady-state creep, and tertiary creep. Here, the steady-state creep of CoCrNi alloy is focused to reveal the creep mechanism. The creep data are analyzed using the following empirical power-law equation [13]:

$$\dot{\varepsilon}_{ss} = A_n \sigma^n \exp\left(-\frac{Q}{RT}\right) \quad (1)$$

where A_n is a material constant, n is the stress exponent, Q is the apparent activation energy, R is the gas constant, and T is the absolute temperature. In order to obtain the value of stress exponent and activation energy Q, according to Equation (1), the dependence of the steady-state strain rate $\dot{\varepsilon}_{ss}$ of CoCrNi alloy on the applied stress σ at various temperatures on a double logarithmic scale and the reciprocal of the absolute temperatures (1/T) at a stress level of 70 MPa on a semi-logarithmic scale are shown in Fig. 2(b and c). The value of the stress exponent of CoCrNi alloy varies in the range of 4.8–5.5, which decreases slightly with the increasing temperature. The calculated average energy Q is about 370 kJ/mol. In order to eliminate the effect of temperature on the determination of the stress exponent, the correlation between normalized creep rates $\frac{\dot{\varepsilon}}{e^{-\frac{Q}{RT}}}$ versus the normalized applied stresses σ/G is plotted in Fig. 2(d), where activation energies Q were taken to be 370 kJ mol^{-1} and the shear modulus $G = 93.6 - 11.9/\left(e^{\frac{362}{T}} - 1\right)$ with the unit of GPa [14]. Obviously, almost all data at different temperatures collapse onto a single line with a slope of 5.3 ± 0.2.

Instead of Eq. (1), the stress-dependence of the steady-state creep rate can also be represented by a stress-assisted thermally activated process,

$$\dot{\varepsilon}_{ss} = \dot{\varepsilon}_0 exp\left(-\frac{H - \sigma V^*}{kT}\right)$$

where k is the Boltzmann's constant, and the activation volume, V*, can be evaluated from

$$V^* = \sqrt{3}kT\left(\frac{\partial ln\dot{\varepsilon}_{ss}}{\partial \sigma}\right) \quad (2)$$

Fig. 2(e) exhibits the values of V* at different temperatures derived from the current creep tests, tensile tests with variable strain rates [11], and strain rate jump tests [11], where b is the Burgers vector length, about 2.52 × 10^{-10} m [11].

3.3. Crept microstructure

To study the microstructural evolution during creep deformation, the crept specimen under 70 MPa at 973 K is selected. The BSE-SEM image of a crack and corresponding EDS results are shown in Fig. 3(a–d). The plate-like precipitates, noted as the gray areas in the SEM image, are observed along the crack. The EDS results indicate these precipitates are Cr-rich phase containing more than 50 atomic percent (at.%) Cr (Cr = ~56.45 at.%, Co = ~19.65 at.%, and Ni = ~23.9 at.%). Meanwhile, the EDS measurement also shows the composition of the alloy matrix near these intergranular precipitates is also different from that of undeformed

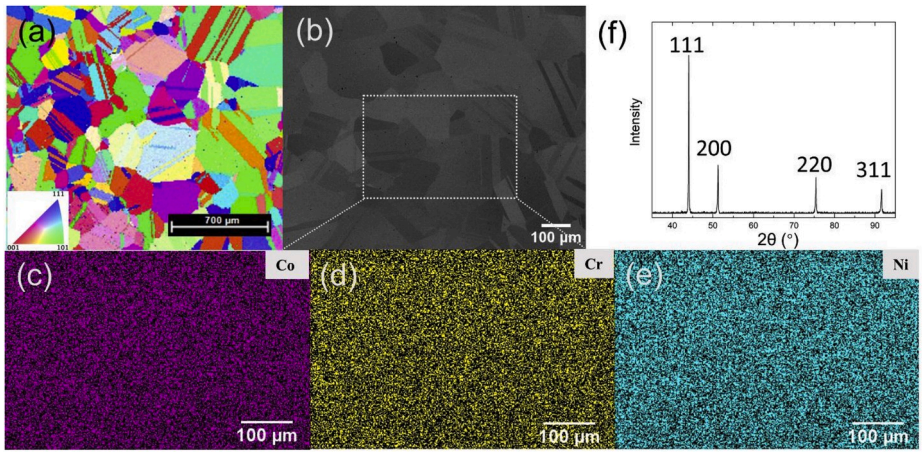

Fig. 1. The initial microstructure of CoCrNi alloy after annealing at 1100 °C for 2 h. (a) Electron backscattered diffraction (EBSD) image, (b–e) BSE-SEM image and EDS elemental maps corresponding to the rectangular area marked in the BSE-SEM image, and (f) X-ray diffraction pattern.

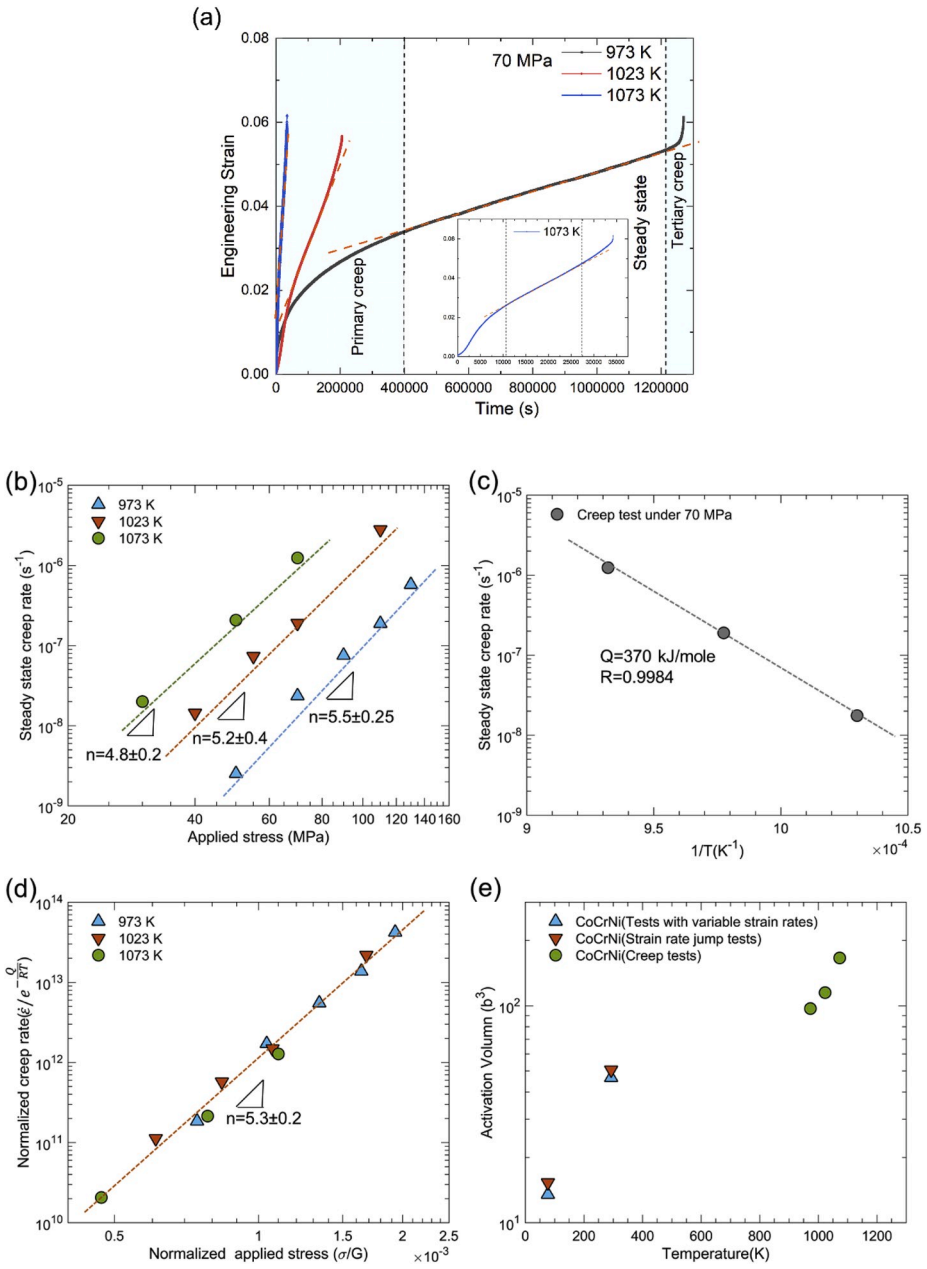

Fig. 2. (a) Selected creep strain-time curves at 70 MPa, (b) Dependence of the steady-state strain rate $\dot{\varepsilon}$ on the applied stress σ at the various temperatures on a double logarithmic scale, (c) Dependence of the steady-state strain rate $\dot{\varepsilon}$ on the reciprocal of the absolute temperatures 1/T at 70 MPa on a semi-logarithmic scale, (d) Dependence of the normalized creep rates on the normalized applied stresses, and (e) The activation volume measured from the creep tests, tensile tests with variable strain rate [11], and strain rate jump tests [11] in the unit of b^3 of CoCrNi alloy.

alloy, with a chemical composition of ~27.37 at.% Cr, ~37.67 at.% Co, and ~34.96 at.% Ni. Actually these precipitates are found to easily form along grain boundaries. This observation suggests a redistribution of the constituent elements in CoCrNi alloy occurring during the creep test. To have a further insight into the creep deformation mechanism and the decomposition behavior, TEM characterization was conducted. From Fig. 4(a), we can see a large number of dislocations that accumulate and entangle with each other to form an uneven distribution and tend to form cell substructures, indicating a dislocation-meditated deformation mechanism. Meanwhile, the bright-field (BF) image of the lath-shape precipitate is exhibited in Fig. 4(b). Combining the EDS results and the selected area electron diffraction (SAED) patterns of both FCC matrix and Cr-rich precipitate along the [110] zone axis (Fig. 4(c)), the crystal structure of these precipitates is identified as Cr-rich tetragonal σ phase. Challenging the previous belief of CrCoNi alloy as a stable single-phase material, decomposition occurs in CoCrNi alloy during the long-term high-temperature test, which is similar to the case of CoCrFeMnNi after extreme long-time annealing [15]. Thus, the integration of high temperature and loading can accelerate the occurrence of decomposition. Moreover, these intergranular precipitates along grain boundaries may open the possibility for the sites for crack initiation or void nucleation, as shown in Fig. 3(a), which significantly reduce the creep lifetime.

4. Discussion

4.1. Deformation mechanism

The stress exponent is often used as the most direct way to determine the dominant creep mechanism. Sherby and Burke [16] have pointed out that the type of creep behavior in solid solution alloys can be divided into two categories. Those alloys whose creep behavior is similar to pure metals are designated as Class II alloys, which favor the dislocation climb with a stress exponent ~5. Class I alloys display a characteristic power-law exponent approximately equal to 3, which is associated with dislocation glide mechanism. According to the value of stress exponent

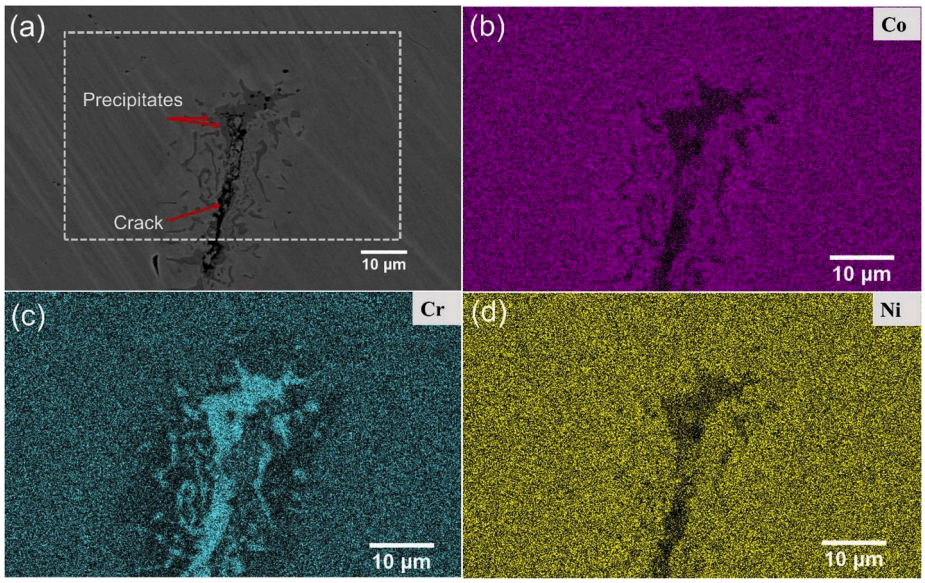

Fig. 3. The microstructure of CoCrNi alloy after creep at 973 K under 70 MPa: (a) BSE-SEM image, (b–d) The corresponding EDS elemental maps.

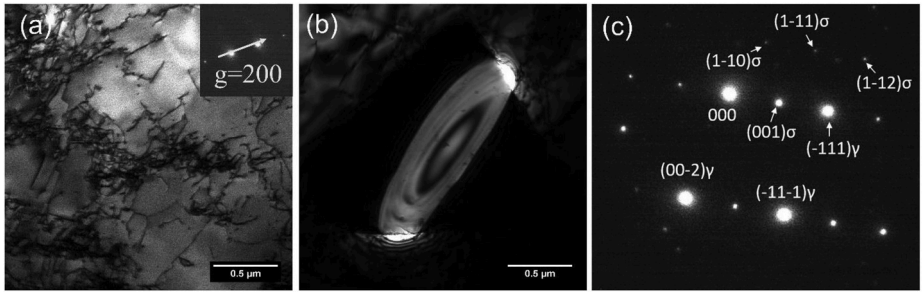

Fig. 4. TEM image of the microstructure formed after creep at 973 K under 70 MPa: (a) Transmission-electron microscope (TEM) images of dislocation substructures, (b) Bright-field (BF) image of the Cr-rich precipitate, and (c) Selected area electron diffraction (SAED) pattern along the [110] zone axis.

n, being 5.3 in our studies, we can conclude CoCrNi solid-solution alloy can be sorted into Class II alloys type with dominated dislocation climb mechanism, the creep behavior of which is more like pure metals. Therefore, the activation energy Q here is the lattice diffusion energy, which is higher than that in CoCrFeMnNi alloy (330 kJ/mol in Ref [17], 268 kJ/mol in Ref. [9], 246 kJ/mol in Ref. [7]). Furthermore, as noted in Fig. 2(e), the activation volume of CoCrNi alloy in this study gradually increases with increasing temperature, ranging from ~100 b^3–~200 b^3. According to the typical range for forest dislocation hardening in FCC materials (~100 b^3 to 1000 b^3) [18], these activation volumes suggest the specific thermally activated motion of dislocation, indicating the dislocation-mediated mechanism during the creep deformation of the CoCrNi alloy.

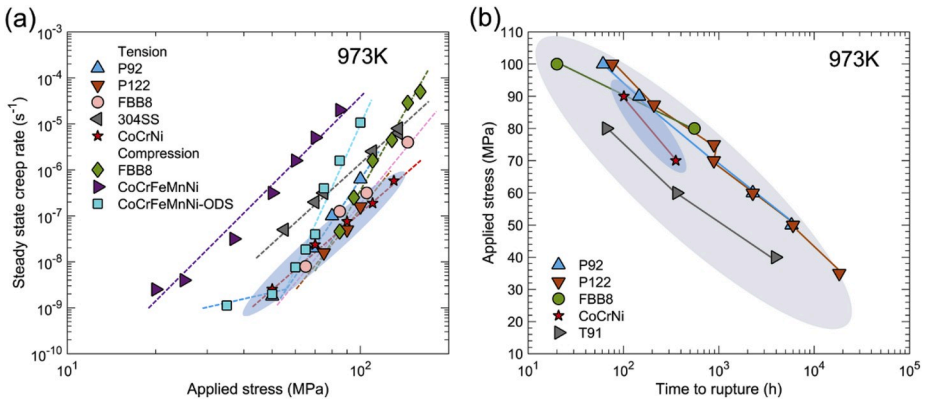

Fig. 5. Comparison of the creep behavior: (a) A plot of the steady-state creep rate versus applied stress for 304 SS [18], commercial ferritic steels (P92, P122, and FBB8) [19–23], CoCrFeMnNi alloy (with/without ODS) [7], and CoCrNi alloy at 973 K, and (b) A plot of the applied stress versus time to rupture for commercial ferritic steels (P92, P122, T91, and FBB8) [19–23], and CoCrNi alloy at 973 K.

4.2. Superior creep behavior

In order to get a direct picture of the creep properties of CoCrNi alloy, the creep resistance (the steady-state creep rate as a function of the applied stress) and creep lifetime with the applied stress at 973 K has been compared with CoCrFeMnNi (grain size 800 nm), oxide-dispersion-strengthened CoCrFeMnNi (CoCrFeMnNi_ODS with grain size 400 nm) [7], 304 stainless steel (SS) [19], and some commercial ferritic steels (P92, P122, T91, and FBB8) [20–23], shown in Fig. 5(a and b). We can see the creep resistance of CrCoNi alloy is comparable to, or even better than, that of some commercial precipitate-strengthened ferritic alloys, and is much better than that of CoCrFeMnNi alloy at the same stress level. The creep lifetime of CoCrNi alloy is also comparable with that of these commercial ferritic steels [20–23] under the same stress level. Note that many of these ferritic steels have complicated hierarchical lath-block microstructures, which nevertheless performs no better than the solid solution CoCrNi alloy.

Since CoCrNi alloy is a subset of CrCrFeMnNi alloy, in this paper, we mainly focus on the difference of the creep resistance in these two alloys. The strain rate caused by the dislocation creep mechanism is independent of the grain size. Although the grain size of CoCrFeMnNi alloy in Ref. [7] is quite different from that of the CoCrNi alloy here, the comparison of the creep behavior in these alloys is still reliable due to the dislocation climb dominated mechanism for these two alloys [7]. At high temperature, nano-twinning induced plasticity and phase transformation become unlikely to be the cause for superior creep resistance of CoCrNi alloy. Also, due to the small amount of the Cr-rich precipitates in CoCrNi alloy, the contribution of dispersion strengthening to creep strength is negligible. Thus, we can assume the two single FCC crystal structure alloys derive all the creep strength from solid solution strengthening.

First, we notice that over a wide range of temperature [11], the flow strength of CoCrNi alloy is much higher than that of CoCrFeMnNi alloy. However, the local lattice distortions in the CoCrNi (0.23%) and CoCrFeMnNi (0.24%) alloys are found to be comparable, originating from chemical short-range order (SRO) and size mismatch effect, respectively [28]. Consequently, the solid solution strengthening alone cannot explain the contrast of creep properties of these two alloys. *Second*, in Class-II solid solution alloys, due to the strong interaction between stacking fault and solute atoms, the solid solution strengthening may be affected by the reduction of stacking fault energy which is associated with the content of alloy composition. The constitutive equation for climb-controlled dislocation creep with the stacking fault energy effect is given in the following form [24]:

$$\dot{\varepsilon}_{ss} = A\left(\frac{\gamma}{Gb}\right)\left(\frac{\gamma}{Gb}\right)^{3}\left(\frac{Gb}{kT}\right)\left(\frac{\sigma}{G}\right)^{5} D_L \tag{3}$$

where D_L is the lattice diffusion coefficient or pipe diffusion coefficient, γ is the stacking fault energy, G the shear modulus, and A is a constant. Apparently, low-stacking-fault energy is an advantage for high creep resistance. Laplanche et al. [25] have measured the stacking-fault energy by means of measuring the partial separations, yielding the value of 22 ± 4 mJ m^{-2} for CoCrNi alloy, which is a quarter lower than that of CrMnFeCoNi (30 ± 5 mJ m^{-2}) [26]. With the solid solution strengthening being the dominant deformation mechanism, the reduction of the stacking fault energy may partly explain why CoCrNi alloy shows a much better creep property than CoCrFeMnNi alloy. *Third*, it should be pointed out that, although the average lattice distortion of this family of alloys is small, the local lattice distortion can be an order of magnitude larger than the average value, thus resulting in large energy barrier against dislocation movement, significant solid-solution strengthening, and sluggish atom diffusion [27]. All these factors are relevant for the high-temperature performance, indicating the severe local lattice distortion, therefore, can contribute to the good creep behavior in CoCrNi and CoCrFeMnNi alloys. Recently, local chemical ordering (LCO) or SRO existing in HEAs was reported, which can affect not only the stacking-fault energy [29], lattice friction [12,30], but also the reduction in diffusivity [31]. Based on the nature of dislocation climb related to the diffusion of vacancy or constituent atoms, consequently, LCO has the potential to affect the dislocation-climb controlled creep performance in these two alloys. Meanwhile, Cr element in this solid solution alloy tends to bond with Ni and Co, forming SRO [32], which suggests a more significant LCO effect in CoCrNi than CoCrFeMnNi alloy due to the higher content of Cr. In this regard, we can speculate the local chemical ordering can have a great influence on the creep behavior in these solid solution alloys. Despite the above findings, it is likely that the effects of LCO may diminish with the increase of temperature because of the homogenization effects of entropy at current test temperatures. Therefore, further experiments, theoretical model and calculations are critically needed.

5. Conclusions

In summary, the creep behavior of CoCrCr alloy at a temperature range of 973–1073 K has been systematically investigated. Like pure metals, the dislocation climb mechanism has been proposed to be the dominant deformation mechanism, with a stress exponent of 5.3 and activation energy 370 kJ/mol. Challenging the previous picture of CoCrNi alloy as single-phase material, Cr-rich σ precipitates are observed along grain boundaries in the fractured samples, indicating the occurrence of decomposition phenomenon in the present alloy during the high temperature creep test. Low stacking fault energy and local chemical ordering in CoCrNi alloy may be the possible reasons for the better creep resistance than that in CoCrFeMnNi alloy. We hope that the creep studies of CoCrNi alloy in this work may shed useful insights into the fundamental understanding of the mechanical properties of HEAs and MEAs.

Declaration of competing interests

The authors declare no competing interests.

CRediT authorship contribution statement

Di Xie: Conceptualization, Data curation, Formal analysis, Writing - original draft. **Rui Feng:** Conceptualization, Data curation, Formal analysis, Writing - original draft. **Peter K. Liaw:** Conceptualization, Data curation, Formal analysis, Writing - original draft. **Hongbin Bei:** Conceptualization, Data curation, Formal analysis, Writing - original draft. **Yanfei Gao:** Conceptualization, Data curation, Formal analysis, Writing - original draft.

Acknowledgements

DX and YG are grateful to the support from the US National Science Foundation (DMR 1809640), and HB to the internal funding from the School of Materials Science and Engineering, Zhejiang University. RF and PKL appreciate the support from the US National Science Foundation (DMR 1611180) and the US Army Research Office under project numbers of W911NF-13-1-0438 and W911NF-19-2-0049.

Appendix A. Supplementary data

Supplementary data to this article can be found online at https://doi.org/10.1016/j.intermet.2020.106775.

References

[1] D.B. Miracle, O.N. Senkov, A critical review of high entropy alloys and related concepts, Acta Mater. 122 (2017) 448–511.
[2] C. Varvenne, G.P.M. Leyson, M. Ghazisaeidi, W.A. Curtin, Solute strengthening in random alloys, Acta Mater. 124 (2017) 660–683.

[3] F. Otto, A. Dlouhý, C. Somsen, H. Bei, G. Eggeler, E.P. George, The influences of temperature and microstructure on the tensile properties of a CoCrFeMnNi high-entropy alloy, Acta Mater. 61 (15) (2013) 5743–5755.
[4] J. Chen, X. Zhou, W. Wang, B. Liu, Y. Lv, W. Yang, D. Xu, Y. Liu, A review on fundamental of high entropy alloys with promising high–temperature properties, J. Alloys Compd. 760 (2018) 15–30.
[5] Y. Yu, F. He, Z. Qiao, Z. Wang, W. Liu, J. Yang, Effects of temperature and microstructure on the triblogical properties of CoCrFeNiNbx eutectic high entropy alloys, J. Alloys Compd. 775 (2019) 1376–1385.
[6] T. Cao, J. Shang, J. Zhao, C. Cheng, R. Wang, H. Wang, The influence of Al elements on the structure and the creep behavior of Al x CoCrFeNi high entropy alloys, Mater. Lett. 164 (2016) 344–347.
[7] F. Dobeš, H. Hadraba, Z. Chlup, A. Dlouhý, M. Vilémová, J. Matějíček, Compressive creep behavior of an oxide-dispersion-strengthened CoCrFeMnNi high-entropy alloy, Mater. Sci. Eng., A 732 (2018) 99–104.
[8] H. Hadraba, Z. Chlup, A. Dlouhy, F. Dobes, P. Roupcova, M. Vilemova, J. Matejicek, Oxide dispersion strengthened CoCrFeNiMn high-entropy alloy, Mater. Sci. Eng., A 689 (2017) 252–256.
[9] C. Cao, J. Fu, T. Tong, Y. Hao, P. Gu, H. Hao, L. Peng, Intermediate-temperature creep deformation and microstructural evolution of an equiatomic FCC-structured CoCrFeNiMn high-entropy alloy, Entropy 20 (12) (2018). Y.B. Kang, S.H. Shim, K. H. Lee, S.I. Hong, Mater. Res. Lett. 6 (2018) 689-695.
[10] Y.B. Kang, S.H. Shim, K.H. Lee, S.I. Hong, Dislocation creep behavior of CoCrFeMnNi high entropy alloy at intermediate temperatures, Mater. Res. Lett. 6 (12) (2018) 689–695.
[11] Z. Wu, Y. Gao, H. Bei, Thermal activation mechanisms and Labusch-type strengthening analysis for a family of high-entropy and equiatomic solid-solution alloys, Acta Mater. 120 (2016) 108–119.
[12] Z. Wu, H. Bei, G.M. Pharr, E.P. George, Temperature dependence of the mechanical properties of equiatomic solid solution alloys with face-centered cubic crystal structures, Acta Mater. 81 (2014) 428–441.
[13] A.K. Mukherjee, J.E. Bird, J.E. Dorn, Experimental Correlations for High-Temperature Creep, 1968.
[14] G. Laplanche, P. Gadaud, C. Bärsch, K. Demtröder, C. Reinhart, J. Schreuer, E. P. George, Elastic moduli and thermal expansion coefficients of medium-entropy subsystems of the CrMnFeCoNi high-entropy alloy, J. Alloys Compd. 746 (2018) 244–255.
[15] F. Otto, A. Dlouhý, K.G. Pradeep, M. Kuběnová, D. Raabe, G. Eggeler, E.P. George, Decomposition of the single-phase high-entropy alloy CrMnFeCoNi after prolonged anneals at intermediate temperatures, Acta Mater. 112 (2016) 40–52.
[16] O.D. Sherby, P.M. Burke, Mechanical behavior of crystalline solids at elevated temperature, Prog. Mater. Sci. 13 (1968) 323–390.
[17] J.Y. He, C. Zhu, D.Q. Zhou, W.H. Liu, T.G. Nieh, Z.P. Lu, Steady state flow of the FeCoNiCrMn high entropy alloy at elevated temperatures, Intermetallics 55 (2014) 9–14.
[18] H. Conrad, Grain size dependence of the plastic deformation kinetics in Cu, Mater. Sci. Eng., A 341 (1–2) (2003) 216–228.
[19] O.K. Chopra, K. Natesan, Interpretation of high-temperature creep of type 304 stainless steel, Metall. Trans. 8 (1977) 633–638.
[20] M. Yoshizawa, M. Igarashi, K. Moriguchi, A. Iseda, H.G. Armaki, K. Maruyama, Effect of precipitates on long-term creep deformation properties of P92 and P122 type advanced ferritic steels for USC power plants, Mater. Sci. Eng., A 510–511 (2009) 162–168.
[21] G. Song, Z. Sun, L. Li, X. Xu, M. Rawlings, C.H. Liebscher, B. Clausen, J. Poplawsky, D.N. Leonard, S. Huang, Z. Teng, C.T. Liu, M.D. Asta, Y. Gao, D.C. Dunand, G. Ghosh, M. Chen, M.E. Fine, P.K. Liaw, Ferritic alloys with extreme creep resistance via coherent hierarchical precipitates, Sci. Rep. 5 (2015), 16327.
[22] W. Zhang, X. Wang, Y. Wang, X. Yu, Y. Gao, Z. Feng, Type IV failure in weldment of creep resistant ferritic alloys: I. Micromechanical origin of creep strain localization in the heat affected zone, J. Mech. Phys. Solid. 134 (2020).
[23] W. Zhang, X. Wang, Y. Wang, X. Yu, Y. Gao, Z. Feng, Type IV failure in weldment of creep resistant ferritic alloys: II. Creep fracture and lifetime prediction, J. Mech. Phys. Solid. 134 (2020).
[24] B. Burton, The influence of stacking fault energy on creep, Acta Metall. 30 (5) (1982) 905–910.
[25] G. Laplanche, A. Kostka, C. Reinhart, J. Hunfeld, G. Eggeler, E.P. George, Reasons for the superior mechanical properties of medium-entropy CrCoNi compared to high-entropy CrMnFeCoNi, Acta Mater. 128 (2017) 292–303.
[26] N.L. Okamoto, S. Fujimoto, Y. Kambara, M. Kawamura, Z.M. Chen, H. Matsunoshita, K. Tanaka, H. Inui, E.P. George, Size effect, critical resolved shear stress, stacking fault energy, and solid solution strengthening in the CrMnFeCoNi high-entropy alloy, Sci. Rep. 6 (2016), 35863.
[27] H. Oh, D. Ma, G. Leyson, B. Grabowski, E. Park, F. Körmann, D. Raabe, Lattice distortions in the FeCoNiCrMn high entropy alloy studied by theory and experiment, Entropy 18 (9) (2016).
[28] Y. Tong, K. Jin, H. Bei, J.Y.P. Ko, D.C. Pagan, Y. Zhang, F.X. Zhang, Local lattice distortion in NiCoCr, FeCoNiCr and FeCoNiCrMn concentrated alloys investigated by synchrotron X-ray diffraction, Mater. Des. 155 (2018) 1–7.
[29] J. Ding, Q. Yu, M. Asta, R.O. Ritchie, Tunable stacking fault energies by tailoring local chemical order in CrCoNi medium-entropy alloys, Proc. Natl. Acad. Sci. U. S. A 115 (36) (2018) 8919–8924.
[30] Q.J. Li, H. Sheng, E. Ma, Strengthening in multi-principal element alloys with local-chemical-order roughened dislocation pathways, Nat. Commun. 10 (2019) 3563.
[31] T. Egami, Structural relaxation in amorphous alloys-compositional short range ordering, Mater. Res. Bull. 13 (6) (1978) 557–562.
[32] F.X. Zhang, S. Zhao, K. Jin, H. Xue, G. Velisa, H. Bei, R. Huang, J.Y.P. Ko, D. C. Pagan, J.C. Neuefeind, W.J. Weber, Y. Zhang, Local structure and short-range order in a NiCoCr solid solution alloy, Phys. Rev. Lett. 118 (20) (2017), 205501.